WILEY | Hindawi

Research Article

Model-Based ILC with a Modified Q-Filter for Complex Motion Systems: Practical Considerations and Experimental Verification on a Wafer Stage

Fazhi Song [iD],[1,2] **Yang Liu** [iD],[1,2] **Jun Cao,**[3] **Li Li,**[1] **and Jiubin Tan**[1]

[1]*Ultra-Precision Optoelectronic Instrumentation Engineering Center, Harbin Institute of Technology, Harbin, China*
[2]*Department of Control Science and Engineering, Harbin Institute of Technology, Harbin, China*
[3]*School of Automation, Harbin Engineering University, Harbin, China*

Correspondence should be addressed to Yang Liu; hitlg@hit.edu.cn

Iterative learning control (ILC) is one of the most popular tracking control methods for systems that repeatedly execute the same task. A system model is usually used in the analysis and design of ILC. Model-based ILC results in general in fast convergence and good performance. However, the model uncertainties and nonrepetitive disturbances hamper its practical applications. One of the commonly used solutions is the introduction of a low-pass filter, namely, the Q-filter. However, it is indicated in this paper that the existing Q-filter configurations compromise the servo performance, although improving the robustness. Motivated by the combination of performance and robustness, a novel Q-filter configuration in ILC is presented in this paper. Some practical considerations, such as the configuration of ILC in a feedback control system, the time delay compensation, and the learning coefficient, are provided in the implementation of the proposed ILC algorithm. The effectiveness and superiority of the proposed ILC versus existing Q-filter ILC are demonstrated by both theoretical analysis and experimental verification on a wafer stage.

1. Introduction

High-performance motion is typically required in many manufacturing environments [1–4] where a tool must track a prescribed reference trajectory with high speed as well as high accuracy. One of the examples is the wafer stage which is responsible for the precision positioning of the wafer used in the IC (integrated circuit) manufacturing. The wafer stage performs a constant velocity scanning during exposure, after which acceleration takes place to bring the stage to the next exposure position [5]. In the next-generation photolithography, the wafer stage is subject to tightening requirements on the servo performance due to larger throughput and smaller critical dimension [6]. However, feedback controllers such as the PID controller alone cannot achieve these requirements due to the closed loop bandwidth limitation from mechanical resonances and electrical amplifiers [7, 8]. More and more efforts are thus devoted to feedforward control techniques.

Considering the repetitive nature of wafer scanning, it is natural to seek to incorporate the information from previous iterations somehow into the control command of the current iteration for the sake of eliminating the recurring servo error. As one such algorithm, iterative learning control (ILC) has found widespread applications in trajectory tracking and disturbance rejection [9–12] since it was initially proposed by Uchiyama [13] and Arimoto et al. [14]. For instance, an iterative learning controller achieves about 93% improvement over the feedback controller in terms of the tracking accuracy in the wafer stage described in [15].

The early work on ILC focused on the design of a single learning filter (called L filter). It uses one gain times the error from the last iteration to update the control input as follows:

$$u^{j+1}(k) = u^j(k) + L(q)e^j(k), \tag{1}$$

where the superscript j denotes the iteration index, k denotes the discrete time index defined on the interval $[0\ N-1]$,
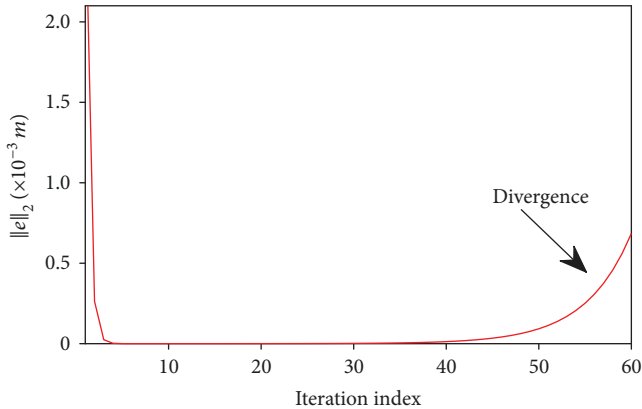
Figure 1: The phenomenon of initial convergence followed by divergence in ILC with only a learning filter.

q represents the forward time-shift operator, u is the control input, e is the error signal, and $L(q)$ is the learning filter.

The ILC algorithm in (1) seems to be very effective from a mathematical perspective and can converge to the zero-tracking error [16]. However, in practice, it usually exhibits unacceptable learning performance, as illustrated in Figure 1. This can be explained by the following:

(1) Most of the ILC algorithms like frequency-domain ILC [17], optimal ILC [18], and so on are to a certain extent model based from the perspective of convergence conditions and performance properties. However, it is intractable in practice to obtain the accurate system model, especially at high frequencies. Frequency domain analysis reveals that the robustness of (1) to model uncertainty is limited [19]. The poor robustness would lead to initial convergence followed by divergence or instability when high frequencies propagate through iterations. (See [20] for more discussion of this phenomenon from several points of view.)

(2) Although attenuating the repetitive disturbances, ILC leads to propagation of noise and nonrepetitive disturbances which could degrade the servo performance [21].

For the improvement of ILC robustness, it is recommended to use a low-pass filter to prevent the high frequencies and noise from entering the learning feedback loop [22, 23]. The widely used ILC algorithm is given as follows:

$$u^{j+1}(k) = Q(q)\left[u^j(k) + L(q)e^j(k)\right], \qquad (2)$$

where $Q(q)$ is the low-pass filter, often called the Q-filter. The Q-filter restricts the bandwidth of the learning process, thereby avoiding the propagation of high frequencies.

Remark 1. For a system with relative degree m, define $L_0(q) = q^{-m}L(q)$; then the ILC algorithm in (2) can be written as $u^{j+1}(k) = Q(q)[u^j(k) + L_0(q)e^j(k+m)]$ which is an equivalently popular ILC formulation as (2) [24].

The design of the Q-filter in (2) has been addressed in numerous literature. In [25], a nonparametric Q-filter which has no requirement on any explicit properties of nonrepetitive disturbances is developed. A zero-phase Q-filter is designed to eliminate the bad learning transient in [16] where, however, it is indicated that the ILC algorithm in (2) leads to a trade-off between robustness and performance. More clearly, a Q-filter with high bandwidth results in improved performance but at the expense of robustness, and vice versa. Although the time-varying Q-filters in [22, 26, 27] and the nonlinear Q-filters in [28] extend the robustness and performance boundaries given by the fixed Q-filter in [16], the ILC algorithms in the form of (2) cannot converge to zero-tracking error unless $Q(q) = 1$ [24]. This motivates the following work in the paper:

(1) Three different ILC configurations under the two DOF (degree of freedom) control architecture are compared in terms of both theoretical analysis and practical considerations.

(2) A novel Q-filter configuration in model-based ILC is proposed. It adjusts the control input utilizing the filtered error signal along with the original control signal from the previous iteration, rather than the filtered one as in (2). The proposed algorithm provides improved performance (zero-tracking error) versus the Q-filter configuration in (2) while maintaining high robustness.

(3) Some additional considerations, such as the zero-phase filter design, time delay compensation, and the learning coefficient, are provided in the implementation of the proposed ILC algorithm.

The rest of the paper is organized as follows: Section 2 describes the wafer stage considered in this paper, followed by its modelling. Section 3 presents the proposed model-based ILC algorithm with a novel Q-filter configuration. In addition, some considerations in the practical implementation are given. In Section 4, experimental results are provided to validate the effectiveness and superiority of the proposed algorithm. Concluding remark is finally given in Section 5.

2. Application Context

2.1. Wafer Stage. In order to reduce the overhead time created by wafer exchange, thereby improving throughput, two wafer stages are used during wafer scanning. While the first stage performs overhead activities such as wafer unload/load, horizontal alignment, and measurement of the surface topography, the second one exposes the previously measured wafer [29]. When both stages are finished with their tasks, the stages are swapped and a new cycle begins. As shown in Figure 2, each of the stages consists of two modules: a long-stroke module and a short-stroke module. The former used for coarse positioning has an H-bridge design, the work range of which is 400 mm with micrometer-level positioning accuracy. The latter is responsible for fine positioning with a 2 mm work range and nanometer-level positioning accuracy.
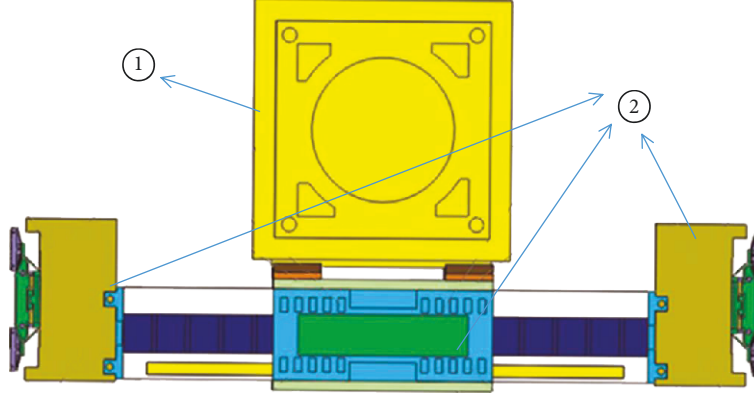
FIGURE 2: Wafer stage. ① short-stroke module; ② long-stroke module.

The wafer stage is controlled in six logical axes: three translations: x, y, and z, and three rotations: r_x, r_y, and r_z. The control system adopts a 6-degree of freedom (DOF) controller structure in combination with force and measurement decoupling designs. Scanning of every field on a wafer is performed in the y-direction by conducting a series of point-to-point motions with constant velocity. After an exposure scan, simultaneous x and y accelerations bring the stage to the next exposure position. Motion in the xy-plane enables the full wafer exposure. Motions in z, r_x, r_y, and r_z are used to keep the wafer surface in the focal plane of the lens. In this paper, for reasons of clarity, only the x-direction long-stroke module is considered. This choice is rather arbitrary but basically captures features that also exist in the remaining directions.

2.2. Modelling. The frequency response of the x-direction long-stroke wafer stage is measured by a sine sweep experiment with a sampling time $T_s = 200\,\mu s$. A series of sinusoidal input signals in the range from 1.0 Hz to 1000 Hz are injected to the stage. The amplitude gain and phase shift are measured by comparing the discrete Fourier transforms of the position and the control signal. Figure 3 shows the measured frequency characteristic, from which it can be observed that the long-stroke wafer stage can be modeled as a double-integrator-based system with a mass of approximately 23.85 kg, in series connection with several resonances at high frequencies. These resonances characterize the structural flexibilities of the stage. In addition, the phase decline below $-180°$ indicates the existence of time delay due to several sources such as the actuator system and current control circuits.

By considering the rigid mode, vibration modes, and the time delay component, the following $P(s)$ can be formulated as the model of the wafer stage:

$$P(s) = K_t \left(\frac{1}{Ms^2} + \sum_{i=1}^{2} \frac{K_i}{s^2 + 2\zeta_i \omega_i s + \omega_i^2} \right) e^{-T_d s}, \qquad (3)$$

where K_t is the gain including the torque constant and amplifier with current control, M is the mass of the wafer stage, K_i
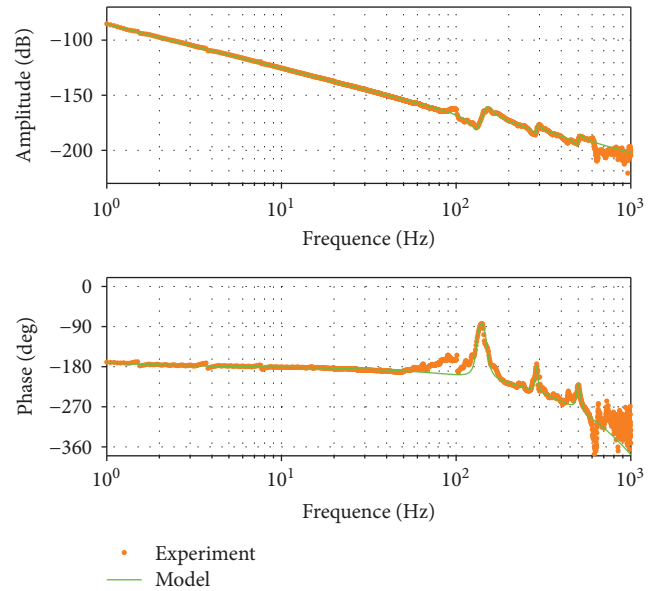

FIGURE 3: Frequency response functions in Bode representation of the x-direction long-stroke wafer stage.

TABLE 1: Parameters in the wafer stage model.

Parameter	Value	Parameter	Value	Parameter	Value
K_t	1/20	M	23.85	T_d	580 μs
K_1	0.0130	ζ_1	0.040	ω_1	$2\pi \times 150$ rad/s
K_2	0.0023	ζ_2	0.018	ω_2	$2\pi \times 292$ rad/s
K_3	0.0038	ζ_3	0.027	ω_3	$2\pi \times 510$ rad/s

is the modal constant of the ith vibration mode, ω_i is the natural angular frequency, ζ_i is the damping coefficient, and T_d is the delay time.

Table 1 lists the parameters in $P(s)$, while the solid curves in Figure 3 show the frequency response of $P(s)$.
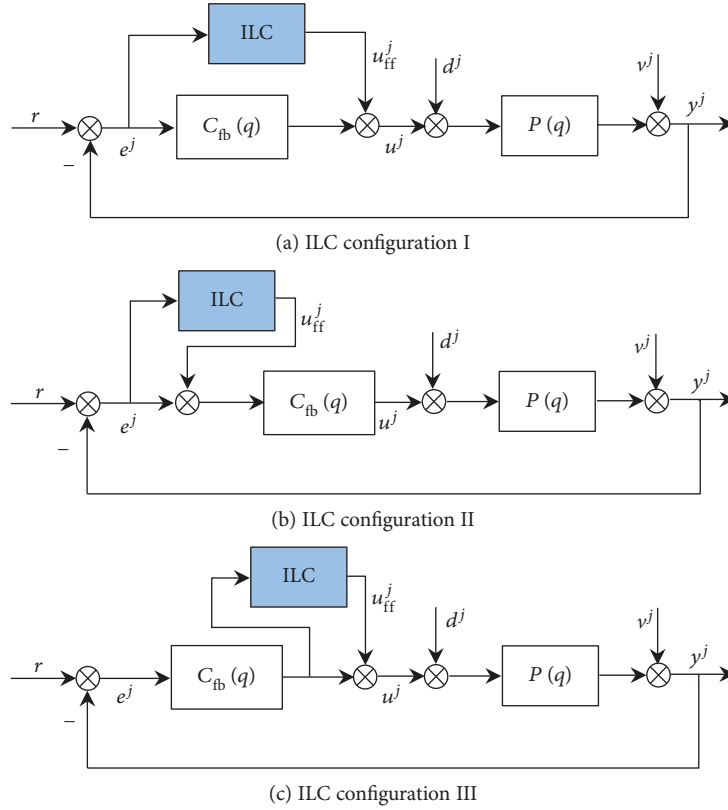
(a) ILC configuration I

(b) ILC configuration II

(c) ILC configuration III

FIGURE 4: Two DOF control structures with different ILC configurations.

3. Model-Based ILC with a Modified Q-Filter

In this paper, the learning filter L and the Q-filter are designed separately although they can be simultaneously designed in some one-step procedures [30]. This kind of ILC design procedure is usually referred to as a two-step ILC design [26]. Note that the following developments are presented in the frequency domain using the z-domain presentation. The z-transformation of a system can be obtained by replacing q with z. The frequency response is given by replacing z with $e^{i\theta}$ for $\theta \in [-\pi\pi]$. Hereafter, the argument of z will be omitted for compactness of notation.

3.1. ILC Configurations. Since ILC is incapable of attenuating the nonrepetitive disturbances, a two DOF control structure is typically used in practice, where ILC is integrated into an existing closed-loop system as an add-on scheme. Based on the choice of (1) *the learning signal* and (2) *the injection point* of the learned control signal, three alternative ILC configurations are usually adopted in precision motion systems [31]. They are illustrated in Figure 4 where C_{fb} denotes the feedback controller designed in advance, u_{ff} is the control effort learned by ILC, e is the error signal, and d and v denote the input and output disturbance of the plant, respectively.

In configurations I [32] and II [25], the learning signal used in ILC is the tracking error, that is, $r - y^j$. The learned control signal u_{ff}^j in configuration I is injected to the input of the plant, whereas the one in configuration II is injected to the input of the feedback controller. In configuration III [31], the learning signal is $C_{fb}(r - y^j)$, and the learned control signal is injected into the input of the plant. In general, the ILC algorithms involved in the configurations can be given as follows, respectively:

$$
\begin{aligned}
&\text{Configuration I:} \\
&u_{ff}^{j+1} = u_{ff}^j + Le^j, \quad u^j = u_{ff}^j + C_{fb}e^j. \\
&\text{Configuration II:} \\
&u_{ff}^{j+1} = u_{ff}^j + Le^j, \quad u^j = C_{fb}\left(u_{ff}^j + e^j\right). \\
&\text{Configuration III:} \\
&u_{ff}^{j+1} = u_{ff}^j + LC_{fb}e^j = u_{ff}^j + C_{fb}e^j.
\end{aligned}
\tag{4}
$$

The analysis and comparison of three ILC configurations are performed in the following.

(a) ILC configuration I

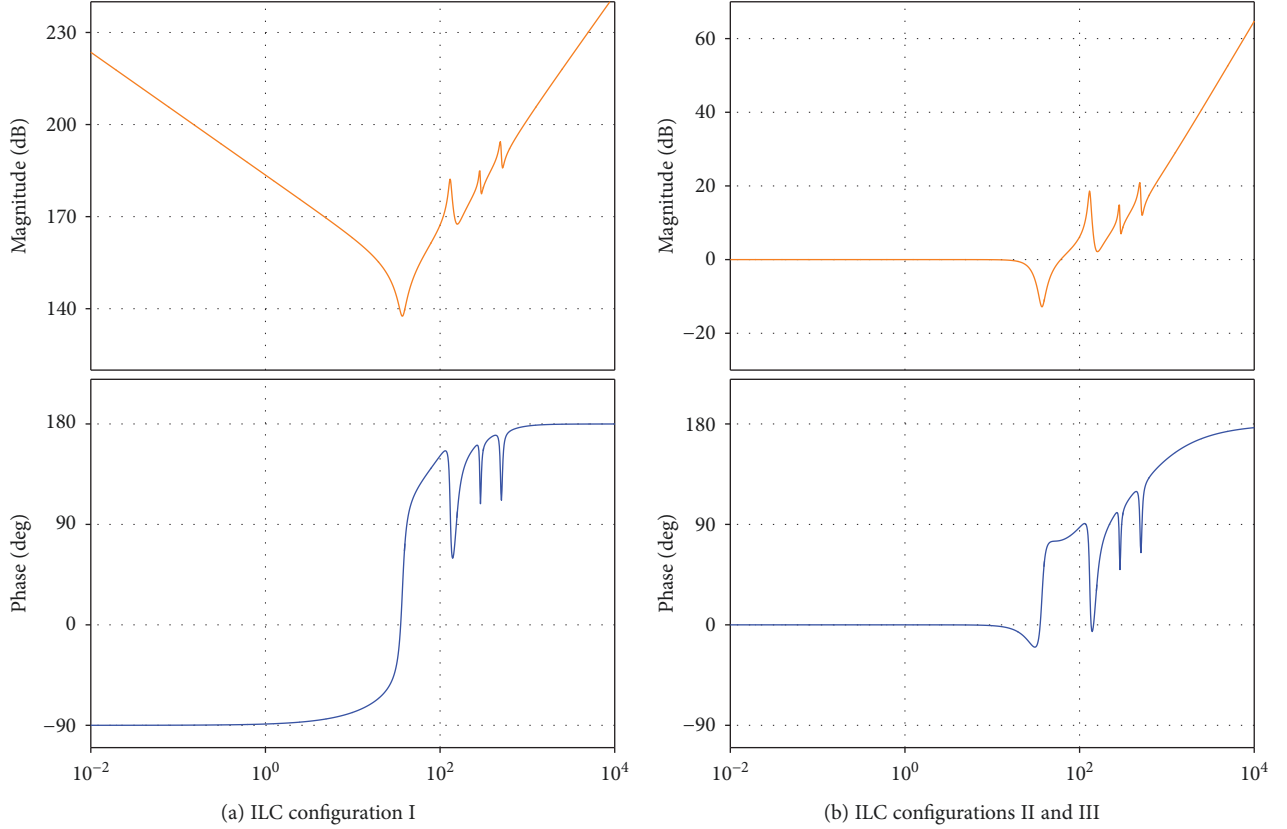(b) ILC configurations II and III

Figure 5: Frequency responses of ideal learning filters for ILC configurations I, II, and III.

3.1.1. Theoretical Analysis. Simple derivations reveal the tracking error propagation from the iteration j to the iteration $j + 1$ as follows:

Configuration I:

$$e^{j+1} = \left(1 - \frac{P}{1 + PC_{\text{fb}}} L\right) e^j - \frac{P}{1 + PC_{\text{fb}}} \left(d^{j+1} - d^j\right)$$
$$- \frac{1}{1 + PC_{\text{fb}}} \left(v^{j+1} - v^j\right).$$

Configuration II:

$$e^{j+1} = \left(1 - \frac{PC_{\text{fb}}}{1 + PC_{\text{fb}}} L\right) e^j - \frac{P}{1 + PC_{\text{fb}}} \left(d^{j+1} - d^j\right) \quad (5)$$
$$- \frac{1}{1 + PC_{\text{fb}}} \left(v^{j+1} - v^j\right).$$

Configuration III:

$$e^{j+1} = \left(1 - \frac{PC_{\text{fb}}}{1 + PC_{\text{fb}}} L\right) e^j - \frac{P}{1 + PC_{\text{fb}}} \left(d^{j+1} - d^j\right)$$
$$- \frac{1}{1 + PC_{\text{fb}}} \left(v^{j+1} - v^j\right).$$

From (5), the ideal learning filters for three configurations can be given as follows, respectively:

Configuration I:

$$L^* = \left(\frac{P}{1 + PC_{\text{fb}}}\right)^{-1}.$$

Configurations II and III:

$$L^* = \left(\frac{PC_{fb}}{1 + PC_{fb}}\right)^{-1}.$$

$$(6)$$

From (6), it seems that there is no difference between the three ILC configurations since each of them can achieve zero convergence rate with the ideal learning filter. However, from the frequency characteristics of the ideal learning filters shown in Figure 5, it can be observed that configurations II and III are well suited for the frequency domain design since the DC gain of the learning filter is close to 1, whereas the DC gain in configuration I tends to be infinite, which may lead to numerical issues.

3.1.2. Practical Considerations. From an implementation point of view, the choice of ILC configurations depends firstly on the availability of the control signals. In precision motion systems, commercial amplifiers and motor drivers are usually used. They provide either an open-loop control where the input is a control signal or a closed-loop control where the input is a reference signal. ILC configurations I and III require direct access to the control input of the plant, which is, however, infeasible if a closed-loop commercial controller

is used. The choice of closed-loop controllers will restrict the user from implementing only ILC configuration II. All ILC configurations can be implemented if an open-loop controller is used.

On the other hand, in ILC configurations I and III, if the ILC algorithm yields a large undesired control signal (resulting from the incorrect numerical computation or the unstable ILC algorithm), the direct injection of this signal would saturate even damage the plant. However, this can be avoided in ILC configuration II since the ILC signal will be filtered by the feedback controller C_{fb} before being injected to the plant.

3.2. Learning Filter Design. Based on all the above discussions, for the sake of implementation and safety, ILC configuration II is adopted in this paper. From (6), the model-inversion learning filter is given as follows:

$$L = \left(\frac{PC_{fb}}{1 + PC_{fb}} \right)^{-1}. \tag{7}$$

Remark 2. If the relative degree of the closed-loop system satisfies $l \geq 1$, then the learning filter in (7) will be noncausal. Unlike the usual notion of noncausality, the ILC algorithm with a noncausal learning filter is still implementable in practice because of the availability of the entire data from all previous iterations.

Remark 3. If the learning filter in (7) is unstable which usually happens when sampling a continuous-time system with a fast sampling time [33], model-inverse techniques for nonminimum-phase systems can be adopted, such as the ZPETC method in [34], the ZMETC method in [35], and the noncausal series approximation method in [36]. See [37] for their comparisons.

Remark 4. From Figure 5(b), it can be observed that the learning filter can be approximated by $L = 1$ at low frequencies. This approximation can be used in practice if a Q-filter is well designed. Despite to its popularity, ILC configuration I is more complicated in terms of the calculation of the learning filter $L = \left(P/(1 + PC_{fb}) \right)^{-1}$. This is another reason why we choose ILC configuration II rather than I.

3.3. Preexisting Q-Filter Configuration. As we discussed in Section 1, if only a single learning filter is used in the model-based ILC, divergence or instability may happen as the iteration increases due to the model uncertainty at high frequencies. A Q-filter is thus often introduced to enhance the robustness of the learning process. Referring to ILC configuration II, the Q-filter is usually configured in ILC as follows:

$$u_{ff}^{j+1} = Q\left(u_{ff}^{j} + Le^{j} \right). \tag{8}$$

3.3.1. Convergence. The frequency-domain condition for the convergence of the ILC algorithm in (8) is given as follows:

Theorem 1. *Consider ILC configuration II in Figure 4(b) and the ILC algorithm in (8). The ILC algorithm is convergent if*

$$\left\| Q\left(1 - \frac{PC_{fb}}{1 + PC_{fb}} L \right) \right\|_{\infty} < 1. \tag{9}$$

Proof. From Figure 4(b), the tracking error in the jth iteration can be given as follows:

$$e^{j} = Sr - Gu_{ff}^{j} - PSd^{j} - Sv^{j}. \tag{10}$$

where $S = 1/(1 + PC_{fb})$ is the sensitivity function and $G = PC_{fb}/(1 + PC_{fb})$ is the closed-loop system function.

From (8) and (10), the tracking error in the $(j + 1)$th iteration can be obtained by

$$e^{j+1} = Sr - G\left[Q\left(u_{ff}^{j} + Le^{j} \right) \right] - PSd^{j+1} - Sv^{j+1}. \tag{11}$$

From (10), we have $Gu_{ff}^{j} = Sr - e^{j} - PSd^{j} - Sv^{j}$ substituting which into (11) yields

$$e^{j+1} = Q(1 - GL)e^{j} + (1 - Q)Sr - PS\left(d^{j+1} - Qd^{j} \right) - S\left(v^{j+1} - Qv^{j} \right). \tag{12}$$

The above error propagation indicates that the ILC algorithm in (8) is convergent if

$$\| Q(1 - GL) \|_{\infty} < 1. \tag{13}$$

3.3.2. Performance. Suppose that the input and output disturbances of the system in Figure 4(b) are repetitive. If the ILC algorithm in (8) is convergent, then it follows that from (12).

$$e^{\infty} = Q(1 - GL)e^{\infty} + (1 - Q)Sr - PS(1 - Q)d - S(1 - Q)v. \tag{14}$$

Therefore, the converged tracking error is

$$e^{\infty} = \frac{(1 - Q)S}{1 - Q(1 - GL)} (r - v - Pd). \tag{15}$$

It can be obviously observed that $e^{\infty} = 0$ holds for all r, d, and v, if and only if the ILC algorithm in (8) is converged and $Q = 1$. Therefore, perfect tracking necessitates $Q = 1$ at the cost of robustness. This indicates that the Q-filter configuration in (8) leads to a tradeoff between robustness and performance.

3.4. Proposed Q-Filter Configuration. As discussed in Section 3.3, the existing ILC algorithm in (8) cannot converge to zero-tracking error unless $Q = 1$, which motivates the following ILC algorithm:

$$u_{ff}^{j+1} = u_{ff}^{j} + QLe^{j}. \tag{16}$$

The Q-filter in the proposed algorithm is configured only in the filtering of the error signal.

3.4.1. Convergence. The following theorem presents the convergence condition of the proposed ILC algorithm in (16).

Theorem 2. *Consider ILC configuration II in Figure 4(b) and the ILC algorithm in (16). The ILC algorithm is convergent if*

$$\left\| 1 - \frac{PC_{\text{fb}}}{1 + PC_{\text{fb}}} QL \right\|_{\infty} < 1. \tag{17}$$

Proof. From (5), we can easily get the tracking error propagation from the iteration j to $j + 1$ as follows:

$$e^{j+1} = \left(1 - \frac{PC_{\text{fb}}}{1 + PC_{\text{fb}}} QL \right) e^j - \frac{P}{1 + PC_{\text{fb}}} \left(d^{j+1} - d \right) \\ - \frac{1}{1 + PC_{\text{fb}}} \left(v^{j+1} - v^j \right), \tag{18}$$

from which, it straightforwardly leads to the frequency-domain convergence condition as shown in (17).

3.4.2. Performance. The converged tracking error yielded by the proposed ILC algorithm in (16) can be given as follows under the assumption on the repetitiveness of d and v:

$$e^{\infty} = \left(1 - \frac{PC_{\text{fb}}}{1 + PC_{\text{fb}}} \right) e^{\infty}, \tag{19}$$

which leads to

$$e^{\infty} = 0. \tag{20}$$

The zero asymptotic tracking error indicates that the proposed algorithm achieves perfect tracking performance, meanwhile maintaining the robustness to uncertainties at high frequencies.

3.5. Practical Considerations. In the real implementation of the proposed algorithm (16), some practical aspects should be considered.

3.5.1. Zero-Phase Q-Filter. The Q-filter is used to maintain the convergence for all frequencies even in the face of model uncertainties. Although any low pass filter could be used as the Q-filter, the zero-phase filter is generally preferable in ILC since it allows no phase sacrifice. In [16, 32], a forth-and-back filtering principle is provided to apply a regular low pass filter in a zero-phase manner. In [19], several ways of representing the zero-phase filter are offered using matrices and transforms.

A comparison about the frequency characteristics of a second-order regular Q-filter and a second-order zero-phase Q-filter is illustrated in Figure 6.

3.5.2. Learning coefficient. In practice, more than one iterations may be desired to average out the influence of non-repetitive disturbances and measurement noise, although zero convergence rate can be achieved theoretically. Therefore, the learning filter L is usually multiplied by a coefficient $0 < \gamma < 1$ to reduce the convergence rate, thereby making the
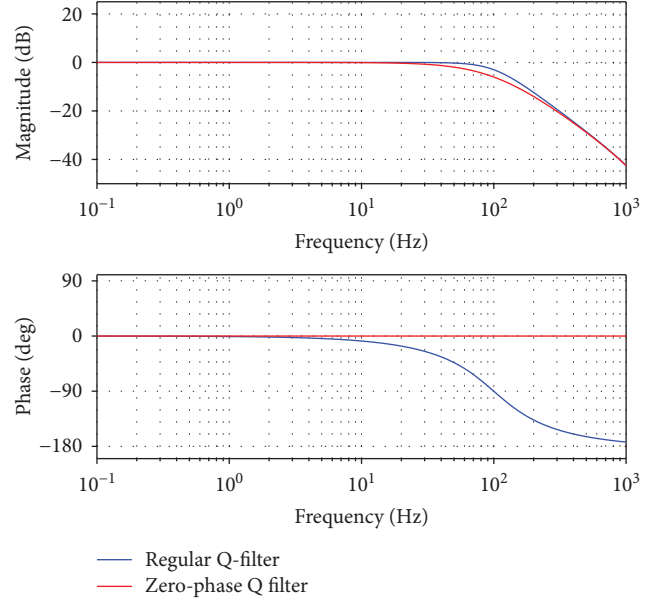

FIGURE 6: Frequency characteristic comparison of regular Q-filter and zero-phase Q-filter.
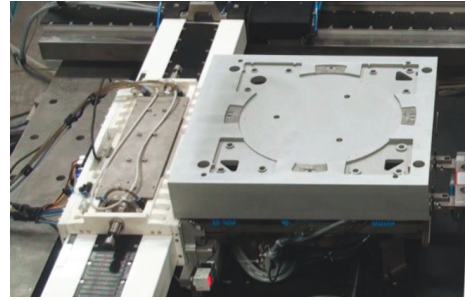

FIGURE 7: Long-stroke wafer stage motion system.

error converge smoothly and averaging out uncertainties through iterations. Note that a large learning coefficient induces fast convergence but is associated with large noise amplification, and vice versa.

3.5.3. Delay Compensator. A time ahead z^{α} is usually incorporated into the ILC controller in order to compensate (1) the relative degree of the system, (2) the time delay resulting from mechanical dynamics, sensors, actuators, and amplifiers as discussed in Section 2.2, and (3) the phase delay caused by the nonzero-phase Q-filter. The proper time ahead is of significant importance to the ILC performance. Insufficient or too much time ahead would lead to slow convergence even divergence.

In summary, the proposed ILC algorithm is presented as follows:

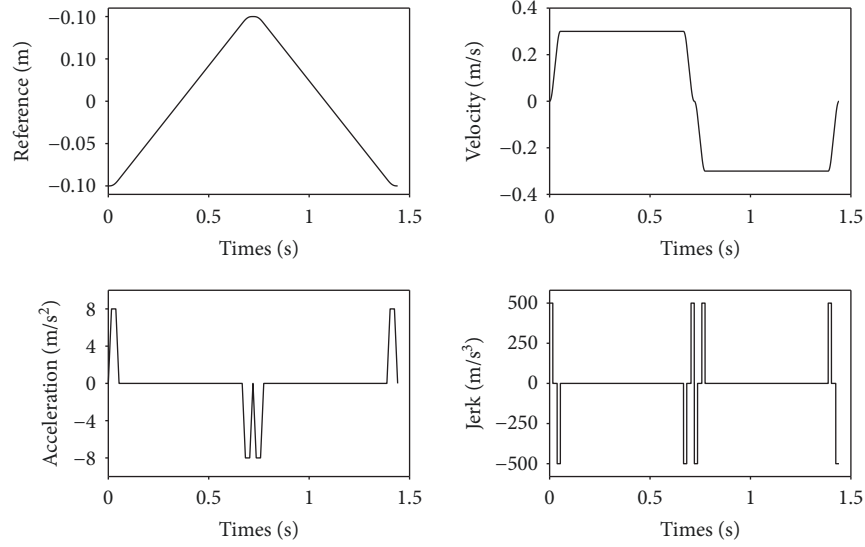$$u_{\text{ff}}^{j+1} = u_{\text{ff}}^j + z^{\alpha} \gamma QLe^j. \tag{21}$$
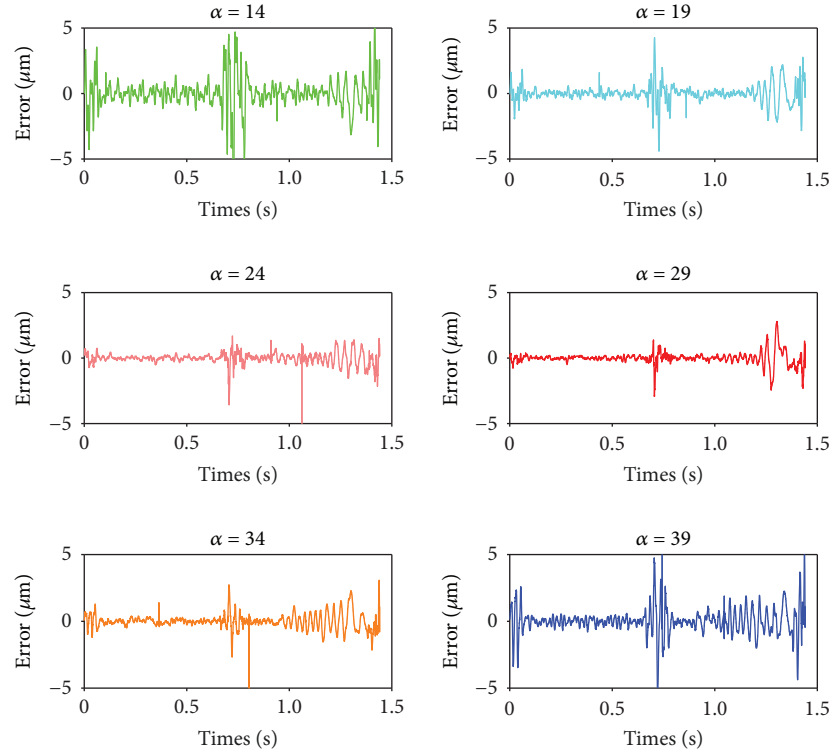
FIGURE 8: Reference trajectory.

FIGURE 9: Converged tracking errors with different times ahead.

Referring to (17), the frequency-domain convergence condition of the ILC algorithm in (21) can be given as follows:

$$\left\| 1 - \gamma z^{\alpha} \frac{PC_{\mathrm{fb}}}{1 + PC_{\mathrm{fb}}} QL \right\|_{\infty} < 1. \tag{22}$$

4. Experimental Verification

In this section, the proposed ILC algorithm in (21) is experimentally validated on a wafer stage as shown in Figure 7.

The wafer stage is mounted on an air bearing with 400 kPa air pressure. The position of the linear motor is measured by a Renishaw linear incremental encoder with the effective resolution of 0.1 μm and maximum velocity of 0.5 m/s. The stage is driven by an all-digital power amplifier based on the field-programmable gate array (FPGA) XC3S400. The bandwidth of the drives is about 2.0 kHz. The wafer stage system is stabilized by a PID feedback controller. The bandwidth of the position loop is about 60 Hz. The drives and the controllers communicate with
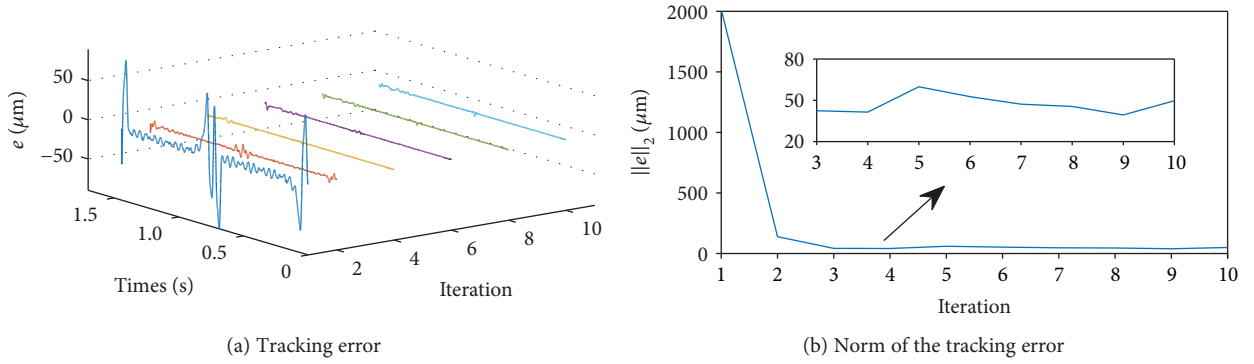
(a) Tracking error

(b) Norm of the tracking error

FIGURE 10: Convergence of the proposed algorithm under $\alpha = 29$.

each other through high-speed fibers. The proposed algorithm is realized by using C language on a TMS320C6414TGLZ DSP controller. The sampling period of the control system is $T_s = 200\,\mu$s. The internal data of the DSP is transmitted to the computer through the network cable and then displayed on the screen.

Although it is a common industrial practice to use a second-order reference trajectory based on a rigid body consideration of a system, high-order motion profiles are more preferred in ultraprecision motion systems since by which less resonant dynamics are excited. In this paper, a third-order polynomial motion trajectory with constraints on the 1st to the 3rd derivatives is used, as shown in Figure 8. It is generated by a trajectory planning algorithm that takes system dynamics into account.

4.1. Effectiveness of the Proposed Algorithm. In the experiments, the learning coefficient γ is set as 0.95, and the following zero-phase Q-filter is used as an alternative to the regular low pass filter.

$$Q = \frac{b_0 + b_1 z^{-1}}{1 + a_1 z^{-1}} \cdot \frac{b_0 + b_1 z}{1 + a_1 z}. \tag{23}$$

where $a_1 = (2 + w_c T_s)/(-2 + w_c T_s)$, $b_0 = b_1 = (w_c T_s)/(-2 + w_c T_s)$, and $w_c = 2\pi \times 100$ is frequency in rad/s.

In order to determine the best time ahead α, experiments with α in the range of 14 to 39 are performed. After convergence, the stable error signals are shown in Figure 9, from which it can be observed that when the time ahead is set as $\alpha = 29$, the best servo performance is achieved. The convergence process is shown in Figure 10. Figure 11 shows the frequency responses of the error propagation functions under $\alpha = 14$, $\alpha = 29$, and $\alpha = 39$. The following indications can be obtained from Figures 10 and 11.

(1) The proposed algorithm is convergent, although the nonrepetitive disturbances and measurement noise could lead to slight fluctuation in the converged error signal.

(2) The learning is most efficient under $\alpha = 29$ since the corresponding error propagation function has the lowest magnitude at each frequency.
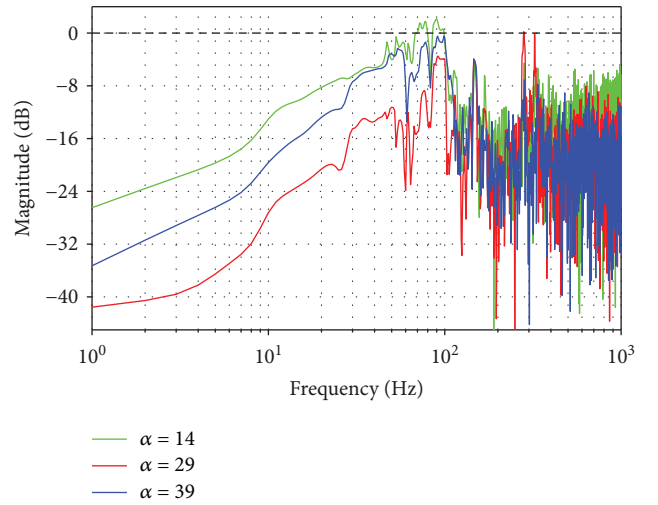

FIGURE 11: Frequency characteristics of error propagation functions under different times ahead.

(3) Insufficient ($\alpha = 14$) or too much ($\alpha = 39$) time ahead would lead to slow convergence even divergence. It can be forecasted that high-frequency errors at about 70 Hz to 100 Hz will be amplified for the learning process with $\alpha = 14$ and divergence would happen as the iteration increases since $\|1 - \gamma z^{\alpha}(PC_{\text{fb}}/(1 + PC_{\text{fb}}))QL\|_{\infty} > 1$.

4.2. Superiority of the Proposed Algorithm. To further verify the high performance of the proposed method, experimental comparison with the existing ILC algorithm in (8) is performed. The Q-filter in (8) is set as the same as the one in (23). The time ahead is set as 29. The tracking error in each iteration is shown in Figure 12, from which the following observations can be obtained:

(1) The conventional ILC algorithm improves robustness against uncertainties, but at the cost of performance. The tracking error converges to $4\,\mu$m during the constant-velocity phase and $20\,\mu$m during the acceleration phase.
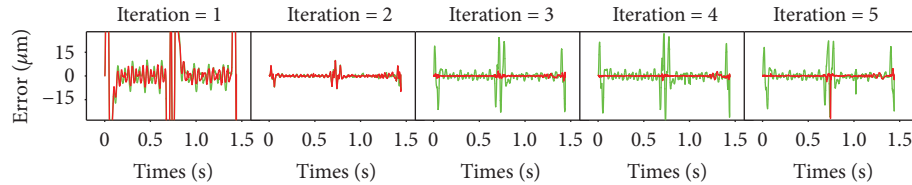
FIGURE 12: Tracking error in each iteration. Red frequency lines: proposed ILC algorithm in (21). Green frequency lines: existing ILC algorithm in (8).

(2) The proposed algorithm in (21) achieves high robustness and high performance simultaneously. The converged tracking errors during the constant-velocity phase and the acceleration phase are $0.25\,\mu m$ and $2\,\mu m$, respectively.

5. Conclusion

In order to deal with the trade-off between servo performance and robustness against model uncertainties in the existing model-based ILC, a novel Q-filter configuration is proposed in this paper. Three commonly used ILC configurations in the two DOF control structure are compared from the perspective of theory and practice. Theoretical analysis reveals the compromise of the existing ILC algorithms on the servo performance. Different from conventional Q-filter configurations, the Q-filter in this proposed ILC algorithm is only configured in the error signal. It avoids the weakening of the control signal and ensures the filtering of the high frequencies in the error signal. Some additional practical considerations are provided when implementing the proposed ILC algorithm. Experimental results confirm the effectiveness and superiority of the proposed method.

The observation in the experimental results that the tracking error in the acceleration phase is always larger than that in the constant-velocity phase would motivate the development of a cut-off frequency-varying Q-filter in the further work.

Data Availability

The data used to support the findings of this study are available from the corresponding author upon request.

Conflicts of Interest

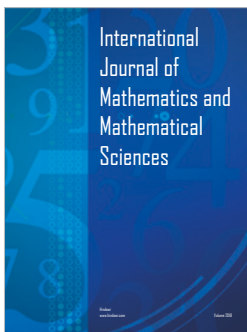The authors declare that they have no conflicts of interest.

Acknowledgments

References

[1] D. A. Bristow and A. G. Alleyne, "A high precision motion control system with application to microscale robotic deposition," *IEEE Transactions on Control Systems Technology*, vol. 14, no. 6, pp. 1008–1020, 2006.

[2] D. J. Hoelzle, A. G. Alleyne, and A. J. Wagoner Johnson, "Basis task approach to iterative learning control with applications to micro-robotic deposition," *IEEE Transactions on Control Systems Technology*, vol. 19, no. 5, pp. 1138–1148, 2011.

[3] J. van Zundert, J. Bolder, S. Koekebakker, and T. Oomen, "Resource-efficient ILC for LTI/LTV systems through LQ tracking and stable inversion: enabling large feedforward tasks on a position-dependent printer," *Mechatronics*, vol. 38, pp. 76–90, 2016.

[4] F. Song, Y. Wang, X. Chen, and P. He, "Research on input shaping algorithm for rapid positioning of ultra-precision dual-stage," in *Proc. SPIE 9556, Nanoengineering: Fabrication, Properties, Optics, and Devices XII*, vol. 9556, pp. 9556P 1–9556P 7, San Diego, CA, USA, 2015.

[5] H. Butler, "Position control in lithographic equipment [applications of control]," *IEEE Control Systems*, vol. 31, no. 5, pp. 28–47, 2011.

[6] T. Oomen, R. van Herpen, S. Quist, M. van de Wal, O. Bosgra, and M. Steinbuch, "Connecting system identification and robust control for next-generation motion control of a wafer stage," *IEEE Transactions on Control Systems Technology*, vol. 22, no. 1, pp. 102–118, 2014.

[7] M. Seron, J. Braslavsky, and G. Goodwin, *Fundamental Limitations in Filtering and Control*, Springer-Verlag, London, U.K, 1997.

[8] T. Oomen, "Advanced motion control for precision mechatronics: control, identification, and learning of complex systems," *IEEJ Journal of Industry Applications*, vol. 7, no. 2, pp. 127–140, 2018.

[9] S. Mishra, J. Coaplen, and M. Tomizuka, "Precision positioning of wafer scanners segmented iterative learning control for nonrepetitive disturbances [applications of control]," *IEEE Control Systems*, vol. 27, no. 4, pp. 20–25, 2007.

[10] S. Mishra, W. Yeh, and M. Tomizuka, "Iterative learning control design for synchronization of wafer and reticle stages," in *2008 American Control Conference*, pp. 3908–3913, Seattle, WA, USA, June 2008.

[11] M. Heertjes and T. Tso, "Robustness, convergence, and lyapunov stability of a nonlinear iterative learning control applied at a wafer scanner," in *2007 American Control Conference*, pp. 5490–5495, New York, NY, USA, July 2007.

[12] M. Heertjes and T. Tso, "Nonlinear iterative learning control with applications to lithographic machinery," *Control Engineering Practice*, vol. 15, no. 12, pp. 1545–1555, 2007.

[13] M. Uchiyama, "Formation of high-speed motion pattern of a mechanical arm by trial," *Transactions of the Society of Instrument and Control Engineers*, vol. 14, no. 6, pp. 706–712, 1978.

[14] S. Arimoto, S. Kawamura, and F. Miyazaki, "Bettering operation of robots by learning," *Journal of Robotic Systems*, vol. 1, no. 2, pp. 123–140, 1984.

[15] F. Song, Y. Liu, J. X. Xu, X. Yang, P. He, and Z. Yang, "Iterative learning identification and compensation of space-periodic disturbance in PMLSM systems with time delay," *IEEE Transactions on Industrial Electronics*, vol. 65, no. 9, pp. 7579–7589, 2018.

[16] H. Elci, R. W. Longman, M. Q. Phan, J.-N. Juang, and R. Ugoletti, "Simple learning control made practical by zero-phase filtering: applications to robotics," *IEEE Transactions on Circuits and Systems I: Fundamental Theory and Applications*, vol. 49, no. 6, pp. 753–767, 2002.

[17] M. Norrlöf and S. Gunnarsson, "Time and frequency domain convergence properties in iterative learning control," *International Journal of Control*, vol. 75, no. 14, pp. 1114–1126, 2002.

[18] J. D. Ratcliffe, J. J. Hätönen, P. L. Lewin, E. Rogers, and D. H. Owens, "Robustness analysis of an adjoint optimal iterative learning controller with experimental verification," *International Journal of Robust and Nonlinear Control*, vol. 18, no. 10, pp. 1089–1113, 2008.

[19] R. Longman, "Iterative learning control and repetitive control for engineering practice," *International Journal of Control*, vol. 73, no. 10, pp. 930–954, 2000.

[20] R. W. Longman and Y.-C. Huang, "The phenomenon of apparent convergence followed by divergence in learning and repetitive control," *Intelligent Automation & Soft Computing*, vol. 8, no. 2, pp. 107–128, 2002.

[21] S. Mishra and M. Tomizuka, "Projection-based iterative learning control for wafer scanner systems," *IEEE/ASME Transactions on Mechatronics*, vol. 14, no. 3, pp. 388–393, 2009.

[22] D. A. Bristow and A. G. Alleyne, "Monotonic convergence of iterative learning control for uncertain systems using a time-varying filter," *IEEE Transactions on Automatic Control*, vol. 53, no. 2, pp. 582–585, 2008.

[23] D. Wang, Y. Ye, and B. Zhang, *Practical Iterative Learning Control with Frequency Domain Design and Sampled Data Implementation*, Springer, Singapore, 2014.

[24] D. A. Bristow, M. Tharayil, and A. G. Alleyne, "A survey of iterative learning control," *IEEE Control Systems*, vol. 26, no. 3, pp. 96–114, 2006.

[25] C. Y. Lin, L. Sun, and M. Tomizuka, "Matrix factorization for design of Q-filter in iterative learning control," in *2015 54th IEEE Conference on Decision and Control (CDC)*, pp. 6076–6082, Osaka, Japan, December 2015.

[26] D. A. Bristow, A. G. Alleyne, and M. Tharayil, "Optimizing learning convergence speed and converged error for precision motion control," *Journal of Dynamic Systems, Measurement, and Control*, vol. 130, no. 5, article 054501, 2008.

[27] D. Yu, Y. Zhu, K. Yang, C. Hu, and M. Li, "A time-varying Q-filter design for iterative learning control with application to an ultra-precision dual-stage actuated wafer stage," *Proceedings of the Institution of Mechanical Engineers, Part I: Journal of Systems and Control Engineering*, vol. 228, no. 9, pp. 658–667, 2014.

[28] M. Heertjes, R. Rampadarath, and R. Waiboer, "Nonlinear Q-filter in the learning of nano-positioning motion systems," in *2009 European Control Conference (ECC)*, pp. 1523–1528, Budapest, Hungary, August 2009.

[29] B. G. Sluijk, T. Castenmiller, R. du Croo de Jongh et al., "Performance results of a new generation of 300-mm lithography systems," in *Proc. SPIE 4346, Optical Microlithography XIV*, vol. 4346, pp. 544–557, Santa Clara, CA, USA, September 2001.

[30] P. Axelsson, R. Karlsson, and M. Norrlöf, "Estimation-based norm-optimal iterative learning control," *Systems & Control Letters*, vol. 73, pp. 76–80, 2014.

[31] H. Hashimoto, P.-H. Yang, K. Hirano et al., "Precision and settling time improvement for the wafer stage of lithography scanners with iterative learning control," in *Proceedings of the 1st International Conference on Positioning Technology*, pp. 91–96, Act-city, Hamamatsu, Japan, 2004.

[32] D. Yu, K. Yang, Y. Zhu, X. Li, and L. Cui, "Nonlinear iterative learning control applied to an aerostatic X–Y planar motion stage," *Proceedings of the Institution of Mechanical Engineers, Part I: Journal of Systems and Control Engineering*, vol. 226, no. 9, pp. 1174–1182, 2012.

[33] K. J. Astrom, P. Hagander, and J. Sternby, "Zeros of sampled systems," *Automatica*, vol. 20, no. 1, pp. 31–38, 1984.

[34] M. Tomizuka, "Zero phase error tracking algorithm for digital control," *Journal of Dynamic Systems, Measurement, and Control*, vol. 109, no. 1, pp. 65–68, 1987.

[35] J. T. Wen and B. Potsaid, "An experimental study of a high performance motion control system," in *Proceedings of the 2004 American Control Conference*, vol. 6, pp. 5158–5163, Boston, MA, USA, USA, June-July 2004.

[36] E. Gross and M. Tomizuka, "Experimental flexible beam tip tracking control with a truncated series approximation to uncancelable inverse dynamics," *IEEE Transactions on Control Systems Technology*, vol. 2, no. 4, pp. 382–391, 1994.

[37] J. A. Butterworth, L. Y. Pao, and D. Y. Abramovitch, "Analysis and comparison of three discrete-time feedforward model-inverse control techniques for nonminimum-phase systems," *Mechatronics*, vol. 22, no. 5, pp. 577–587, 2012.